



Brownian coagulation of like-charged aerosol particlesPijush Patra  and Anubhab Roy ^{*}*Department of Applied Mechanics, Indian Institute of Technology Madras, Chennai 600036, India*

(Received 17 January 2022; accepted 6 June 2022; published 29 June 2022)

In this paper, we study the coagulation rate of like-charged Brownian spherical particles dispersed in a gaseous medium. Most previous calculations of the Brownian-induced coagulation rate have considered that the particle pairs interact through continuum hydrodynamics, and at a close approach, van der Waals attraction forces allow the collision and subsequent coagulation. However, the continuum approximation of the hydrodynamic interactions is no longer valid when the gap thickness between the surface is less than the mean free path of the surrounding fluid medium and the noncontinuum lubrication interactions lead to surface-to-surface contact in a finite time. We report the Brownian coagulation rate in the presence of noncontinuum lubrication resistances for a range of pair size ratios. At small separations, like-charged conducting particles almost always attract each other. Thus we also incorporate the attractive electrostatic interactions between like-charged conducting spheres in our calculation and report the effects of van der Waals and electrostatic forces on the coagulation rate of conducting spheres interacting with each other through noncontinuum hydrodynamics for a range of size and charge ratios.

DOI: [10.1103/PhysRevFluids.7.064308](https://doi.org/10.1103/PhysRevFluids.7.064308)**I. INTRODUCTION**

The coagulation of aerosol particles induced by Brownian motion and modulated by hydrodynamic interactions and interparticle forces plays a vital role in many industrial and environmental processes. Brownian motion is the primary driving force for collisions between smaller particles (radii $1\ \mu\text{m}$ or lesser). In contrast, background turbulence and gravity predominantly drive the collision mechanisms for larger particles [1]. Colloidal suspensions, carbon black in aerosol reactors, soot particles formed by combustion, dust particles in space, and volcanic ash are a few examples of situations where charged particles coagulate due to Brownian diffusion [2]. When air humidity reaches above a deliquesce humidity, aerosol particles grow due to the condensation of water vapor on their surfaces and transform into haze droplets with dissolved ions. At low water vapor pressure, these ions lead to stabilizing the haze droplets to a small size, and then the condensational growth becomes negligible. Thus, in the initial stage of rain formation in warm cumulus clouds, haze droplets grow due to Brownian coalescence [3]. We will focus on dilute systems because particle volume fractions are low [about $O(10^{-6})$] in many natural and industrial systems such as atmospheric clouds [4], and aerosol reactors [5]. For dilute dispersions, the interactions and collisions between more than two particles are highly unlikely, and thus we restrict our analysis to binary interactions as shown in Fig. 1. We assume only hard-sphere interactions between the particles during collisions, and this assumption is also valid for tiny water droplets due to their high drop-to-medium viscosity ratio.

The collision rate between the particles significantly affects the evolution of the particle size distribution. When only two species are present, the rate equation for the particle number density

^{*} Author to whom correspondence should be addressed: anubhab@iitm.ac.in

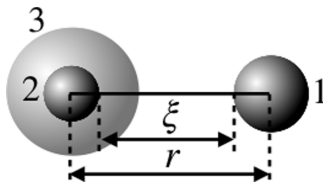


FIG. 1. The schematic representation of binary interactions. “1” indicates the sphere with radius a_1 and surface charge q_1 ; “2” indicates the sphere with radius a_2 and surface charge q_2 . The sphere marked “3” is the collision sphere of radius $a_1 + a_2$. In Sec. II, we will use \hat{e}_r as the unit vector in the radial direction.

can be written as

$$-\frac{dn_1}{dt} = -\frac{dn_2}{dt} = K_{12}, \quad (1)$$

where K_{12} is the rate at which two species of particles with radii a_1 and a_2 and respective number densities n_1 and n_2 coagulate to form a new species. The theoretical prediction for the coagulation rate is challenging, especially when one accounts for the roles of hydrodynamic interactions and/or interparticle forces. Smoluchowski [6] determined the ideal coagulation rate (K_{12}^0) of noninteracting spheres due to Brownian diffusion and found that $K_{12}^0 = 4\pi n_1 n_2 D_0 (a_1 + a_2)$. Here, the relative diffusivity of two noninteracting spheres, $D_0 = k_B T (a_1 + a_2) / (6\pi \mu_f a_1 a_2)$, where $k_B = 1.381 \times 10^{-23} \text{ J K}^{-1}$ is the Boltzmann’s constant, T is the absolute temperature of the dispersion, and μ_f is the dynamic viscosity of the fluid medium. The coagulation between particles depends on the driving forces and the interparticle interactions that significantly alter the relative velocity between the particles at close separations. We will quantify the effects of interparticle interactions on the collision rate through the collision efficiency $E_{12} = K_{12}/K_{12}^0$, which is the ratio of the collision rate in the presence of interactions to that obtained ignoring interactions (the ideal collision rate). Spielman [7] presented a theoretical model to estimate the coagulation rate of two equal-sized rigid spheres subject to Brownian diffusion with continuum hydrodynamic interactions, van der Waals, and electrical double-layer potentials. Valioulis and List [8] and Kim and Zukoski [9] analyzed similar problems for polydisperse rigid spheres. In these studies, the authors calculated the coagulation rate by solving the steady-state diffusion equation describing the relative Brownian motion between particle pairs.

We assume that both the fluid and particle inertia are negligible, and thus the effects of inertia on the collision dynamics are insignificant. Though gravitational settling is negligible for submicron aerosols, both Brownian diffusion and gravitational settling are important for micron-sized particles. The nondimensional quantity Pe , the Peclet number, that defines the relative importance of gravitational sedimentation to Brownian diffusion, is given by [10] $Pe = 2\pi(\rho_p - \rho_f)a_1^4 \kappa(1 - \kappa^2)g / (3k_B T)$, where $\kappa = a_2/a_1 \leq 1$ is the size ratio, and g is the acceleration due to gravity. For Brownian-dominated coagulations $Pe \ll 1$ and gravity-dominated coagulations $Pe \gg 1$. In this study, we assume $Pe \ll 1$ (i.e., gravitational sedimentation is negligible). To validate this assumption, let us compute the quantity Pe for a water droplet in air with $a_1 = 0.5 \mu\text{m}$ (droplet radius), $\rho_p \approx 10^3 \text{ kg m}^{-3}$ (density of water droplet), $\rho_f \approx 1 \text{ kg m}^{-3}$ (density of air), $\mu_f \approx 1.8 \times 10^{-5} \text{ Pa s}$ (dynamic viscosity of air), and $T = 298 \text{ K}$. We found $Pe \approx 0.08$ for $\kappa = 0.3$ and $Pe \approx 0.006$ for $\kappa = 0.99$. So, the above typical values of Pe justify our assumption.

Collision rates between particle pairs depend on the detailed interparticle interactions, both hydrodynamic and colloidal. The continuum assumption of hydrodynamic interactions fails at close separations, and the near-field noncontinuum interactions become the dominant mechanism for collisions in media with long mean free paths [11,12]. The Knudsen number $Kn = \lambda_0/a^*$, where λ_0 is the mean free path of the medium and $a^* = (a_1 + a_2)/2$ is the average radius of the two interacting spheres, measures the strength of noncontinuum effects. The gas pressure p_g is related to the mean free path λ_0 by $\lambda_0 = k_B T / (\sqrt{2}\pi d^2 p_g)$, where d is the molecular diameter of the gas molecule. We

consider $d = 3.7 \times 10^{-10}$ m for air at 298 K. Thus, we can express Kn in terms of particle size, size ratio, and gas pressure as $\text{Kn} = 0.0135/[a_1(1 + \kappa)p_g]$. For $a_1 = 0.5 \mu\text{m}$ and $\kappa = 1$, the Knudsen number Kn decreases from 1.34 to 0.0134 when p_g increases from 0.1 to 10 atm. In this study, we will present our results for Kn spanning from 10^{-1} to 10^{-4} . The purpose behind calculating the collision efficiency for the smallest values of Kn is to establish that even minor noncontinuum hydrodynamics effects can significantly alter the underlying dynamics associated with the pure continuum interaction. However, in an experimental situation, $\text{Kn} = O(10^{-3})$ and smaller would not be accessible in a low-pressure gas medium without increasing the particle size or, in other words, without considering the sedimentation effects. When $\text{Kn} = O(1)$ or higher, the particles undergo a persistent Brownian motion (i.e., without changing their directions, particles move a distance that is comparable to interparticle separation) because they experience lesser drag forces. Several theoretical and experimental studies for the $\text{Kn} \geq O(1)$ scenario are available in the literature [13–18]. The analysis by Sitarski and Seinfeld [14] deserves special mention since it provides a theoretical result for the Brownian coagulation rate over a wide range of particle sizes and thus Kn, connecting Smoluchowski’s continuum result with the rate constant known in the free molecular regime. We consider $\text{Kn} \ll 1$ in the current analysis. In the $\text{Kn} \ll 1$ limit, the persistence distance is much smaller than the interparticle separation, and thus the pair diffusion equation describing the standard Brownian coagulation theory [19] will still be applicable. Noncontinuum effects become significant when $\xi \leq O(\text{Kn})$, where ξ is the nondimensional surface-to-surface distance. Initially, Hocking [20] tried to quantify the noncontinuum effects by applying Maxwell slip boundary conditions for continuum equations in the lubrication gap. Later, Davis [21] estimated the noncontinuum effects for differentially settling spheres using Hocking’s results. However, these calculations are valid only for $\text{Kn} \ll \xi \ll 1$ and thus do not accurately capture the noncontinuum hydrodynamics. For $\xi \leq O(\text{Kn})$, Sundararajakumar and Koch [22] derived the noncontinuum lubrication force by solving the linearized Boltzmann equation for the noncontinuum flow in a channel (a local geometry of the lubrication gap). Utilizing the work of Sundararajakumar and Koch, recently, Dhanasekaran *et al.* [23] calculated the modification of axisymmetric mobilities due to noncontinuum lubrication interactions. This study uses the uniformly valid axisymmetric mobility function developed by them. We will briefly discuss their work in Sec. II B. Previously, Chun and Koch [12] derived an analytical expression for the coagulation rate of two equal-sized Brownian particles as a function of Kn both with and without van der Waals forces. They demonstrated the importance of noncontinuum hydrodynamics interactions by comparing their predicted collision efficiency with experimental measurements of Devir [24,25] who used a modified Sinclair-LaMer generator to produce dioctyl phthalate drops of average radii 0.5–0.8 μm and a Derjaguin counter to determine the time evolution of the number density of aerosols. In the current work, we extend the noncontinuum lubrication analysis for arbitrary-sized particle pairs. Also, our analysis includes an improved treatment for the retarded van der Waals and the addition of electrostatic interaction forces.

The perfect conductor assumption for charged aerosol particles would not hold well because their dielectric constants are finite. The deviation from the perfect conductor behavior is much less for tiny metal particles than for haze droplets. Furthermore, the ions dissolved inside haze drops may alter their dielectric constants. Gavish and Promislow [26] theoretically studied the dependence of the dielectric constant of water in aqueous electrolyte solutions upon the salt concentration and temperature. If applied to representative ion concentrations in cloud droplets [1], their analysis shows that the change in the dielectric constant would be negligible. To reduce the complexity of our current analysis, we assume that the behavior of interacting particles is akin to perfect conductors. We also assume that the concentration of free ions in the surrounding fluid medium is low. Therefore, the potential of electric double-layer repulsion is insignificant and does not influence the Brownian coagulation or coalescence. The calculation of the electrostatic interaction force between two charged conducting spheres has a long history [27]. The method of image charges, the multipole expansion techniques, and the solutions using the bispherical coordinate system are the three popular approaches for calculating the electrostatic interaction force [28]. Among these three approaches, the bispherical coordinates solution offers higher accuracy when the gap between

the conductor is small [29]. Russell [30], and later Lekner [31,32], derived an analytical expression for the electrostatic forces in the lubrication region of two conducting spheres using capacitance coefficients [33,34]. They found that two charged conducting spheres always attract each other at short distances (even when their nature of charges is the same) except for those charge ratio values that the spheres would attain by bringing them into contact. Interestingly, Lekner showed that the attractive force has a $O(\xi^{-1}[\log \xi]^{-2})$ singularity, which grows indefinitely as the separation approaches zero (see also Khair [35] and Banerjee *et al.* [36]). The relation between the size ratio $\kappa = a_2/a_1$ and the charge ratio $\beta = q_2/q_1$ for which the electrostatic interaction force will always be repulsive is [32,37]

$$\beta = \frac{q_2}{q_1} = \frac{\gamma + \psi\left(\frac{a_1}{a_1+a_2}\right)}{\gamma + \psi\left(\frac{a_2}{a_1+a_2}\right)} = \frac{\gamma + \psi\left(\frac{1}{1+\kappa}\right)}{\gamma + \psi\left(\frac{\kappa}{1+\kappa}\right)}, \quad (2)$$

where $\gamma = 0.5772156649\dots$ is the Euler constant and ψ is the digamma function. In the present study, we need the expression for the electrostatic potential energy as a function of separation. We will utilize Lekner's work [31] to obtain the coagulation rate of hydrodynamically interacting aerosols in the presence of electrostatic forces. Khachatourian and Wistrom [38] estimated the enhancement in the coagulation rate due to electrostatic interactions of polydisperse aerosol particles. However, they did not consider the hydrodynamic and van der Waals interactions. Huang *et al.* [39] obtained an enhancement of the Brownian coagulation rate between a charged and an uncharged particle, accounting for an attractive image potential and unretarded van der Waals interaction, across a range of Kn. The study neglected the hydrodynamic interaction between the particles and considered a far-field expansion of the attractive image potential, truncated to the first four terms. Thus when both particles are charged, the leading order Coulombic interaction dominates over the image potential. In our current study, we show that the complete form of the electrostatic field will significantly deviate from a pure Coulombic interaction in the near field, thus considerably altering the collision physics. The effect of the combined electric fields of neighboring charged particles on the collision rate is not straightforward to determine. Even though, as hydrodynamic interactions, electrostatic interactions are also long range and many body in nature, the pair interaction assumption is reasonable to consider for the dilute suspensions [40]. On the other hand, for suspensions with high volume fractions, one must incorporate the influence of all other particles by summing up all the pairwise interactions while solving the particle-phase equations. Recently, Yao and Capecehatro [41] implemented an efficient numerical scheme in an Eulerian-Lagrangian framework for accurately capturing the effects of Coulomb forces of charged inertial particles in a Taylor-Green vortex and an isotropic turbulent flow as a function of the nondimensional parameter called electric settling velocity.

The experiments performed by Devir [25] reported that the average particle charges encountered in their investigation were small ($1e-3e$ per particle with $e = 1.602 \times 10^{-19}$ C being the elementary charge) and that these charges had a negligible effect on the coagulation rate within the accuracy of the measurements. The quantity of electric charge and the maximum amount of charge an aerosol particle of a given size can acquire varies depending on the charging mechanisms. A few of these mechanisms are flame charging, static electrification, diffusion charging, and field charging (see Chap. 15 of Hinds [42] for details). The experimental study of Kousaka *et al.* [43] found that the magnitude of particle charge significantly depends on aerosol materials and generation methods, such as evaporation-condensation, chemical reaction, atomization, and mechanical dispersion. Tsai *et al.* [44] used an aerosol charge analyzer to measure the absolute average charge on atomized NaCl particles. For different initial aqueous concentrations, their experiments found that the absolute quantity of charges on particles with diameters ranging from 0.2 to 1 μm is about $1e-10e$. The experimental investigation of Ghosh *et al.* [45] showed that the aerosol particle size versus average absolute charge [measured by an electrical low-pressure impactor (ELPI)] plot approximately follows the Boltzmann equilibrium charge distribution. The number of elementary charges on soot particles depends on the charging mechanisms, ion concentration (N_i), time duration of charging

(t), and the electric field (E) in the case of field charging. For a particle of radius $0.5 \mu\text{m}$, $q_1 = 42e$ (diffusion charging) and $q_1 = 162e$ (field charging with $E = 500 \text{ kV/m}$) when $N_1 t = 10^{13} \text{ s/m}^3$ (see Hinds [42]). The charges in metal particles or particles produced in flames are typically much less than the Rayleigh, electron, and ion limit charges [42]. Experimental studies also confirm that submicron-sized soot particles carry only a few elementary charges (see Onischuk *et al.* [46] and Maricq [47]). In atmospheric clouds, tiny aerosol particles of radii $0.1\text{--}1.0 \mu\text{m}$ typically carry a few elementary charges ranging from less than $1e$ up to a maximum of $42e$ (see Tinsley *et al.* [48]). Several numerical and experimental studies have investigated the effect of charge on the coagulation rate and the time evolution of the aerosol particles' size distribution [49–52]. However, while solving the number density equation numerically, none of these studies have considered the coagulation rate that accounts for noncontinuum lubrication interactions and appropriate electrostatic and van der Waals potentials between the charged conducting aerosol particles.

We will analyze the collision rate of Brownian spheres interacting through noncontinuum hydrodynamics, van der Waals, and electrostatic forces. In Sec. II A, we will go through the formal derivation of the collision efficiency for Brownian particles [12,53]. The collision efficiency is directly related to the hydrodynamic mobility function and interparticle potential. Subsequently in Sec. II B, we will briefly review the procedure for the noncontinuum corrections of axisymmetric hydrodynamic mobility functions [23]. We will quantify the effects of noncontinuum hydrodynamics, van der Waals, and electrostatic interactions individually and various combinations of these three driving forces in Sec. III. Finally, in Sec. IV, we will summarize our results and discuss possible future works.

II. FORMULATION

A. The expression for the particle collision efficiency

We consider a dilute dispersion with a spectrum of particle sizes and seek to estimate the rate at which particles of radii a_1 and a_2 with number densities n_1 and n_2 collide with each other per unit volume. Mathematically, the collision rate K_{12} is equal to the flux of pairs into the collision sphere of radius $r = a_1 + a_2$ and can be expressed in terms of the pair-distribution function $P(r)$ and the relative velocity \mathbf{V} [21],

$$K_{12} = -n_1 n_2 \int_{(r=a_1+a_2) \text{ and } (\mathbf{V} \cdot \mathbf{n} < 0)} (\mathbf{V} \cdot \mathbf{n}) P dA, \quad (3)$$

where \mathbf{n} is the outward unit normal at the spherical contact surface. The radial component of the relative velocity must be inward at contact for two colliding spheres, or, in other words, $\mathbf{V} \cdot \mathbf{n} < 0$ at $r = a_1 + a_2$. For a dilute dispersion, the pair-distribution function P satisfies the quasisteady Fokker-Planck equation

$$\nabla \cdot (P\mathbf{V}) = 0. \quad (4)$$

We assume colliding aerosols coagulate when they come into contact and so $P = 0$ at $r = a_1 + a_2$. The absence of far-field correlations sets the upstream boundary condition: $P \rightarrow 1$ as $r \rightarrow \infty$.

For submicron aerosols, gravitational sedimentation is negligible, and thus the gravity-induced coagulation is not significant. In this case, the Brownian diffusion and interparticle forces drive the relative motion between the particles. The relative velocity between two particles is given by [53]

$$\mathbf{V} = -\frac{D_0}{k_B T} G \left(\frac{d\Phi}{dr} + K_B T \frac{d \ln P}{dr} \right) \hat{e}_r, \quad (5)$$

where G is the axisymmetric mobility function that captures the effects of hydrodynamic interactions (we will discuss this in detail in Sec. II B), and Φ is the interparticle potential. For the present problem, we can write

$$\Phi = \Phi_{\text{vdW}} + \Phi_{\text{el}}, \quad (6)$$

where Φ_{vdW} and Φ_{el} are the van der Waals and electrostatic potential energy, respectively (see Appendixes A and B for details). Inserting the expression of V from (5) into (4) and then integrating twice we have

$$P = \exp(-\Phi/k_B T) \frac{\int_{a_1+a_2}^r \exp(\Phi/k_B T)/r^2 G dr}{\int_{a_1+a_2}^{\infty} \exp(\Phi/k_B T)/r^2 G dr}. \quad (7)$$

In deriving the expression of P , we apply the condition that both the van der Waals and electrostatic potential energy approach zero at large separation (i.e., $\Phi_{\text{vdW}}, \Phi_{\text{el}} \rightarrow 0$ as $r \rightarrow \infty$). Using the expression of the pair-distribution function and the relative velocity, we perform the integral in (3) to obtain the collision rate per unit volume. Thus the expression for the collision rate becomes

$$K_{12} = 4\pi n_1 n_2 D_0 \left[\int_{a_1+a_2}^{\infty} \frac{\exp(\Phi/k_B T)}{r^2 G} dr \right]^{-1}. \quad (8)$$

From the above expression, we can recover Smoluchowski's result for the ideal coagulation rate (K_{12}^0) due to Brownian motion by setting the interparticle potential $\Phi = 0$ and the hydrodynamic mobility $G = 1$. To simplify the analysis, we scale the interparticle separation r by the average radius $a^* = (a_1 + a_2)/2$. Hereafter, r represents the dimensionless center-to-center distance and can range from 2 (the collision sphere) to ∞ (negligible interactions between the particles). Therefore, the final expression for the collision efficiency is

$$E_{12} = \left[2 \int_2^{\infty} \frac{\exp[(\Phi_{\text{vdW}} + \Phi_{\text{el}})/k_B T]}{r^2 G} dr \right]^{-1} = \left[2 \int_2^{\infty} \frac{\exp(N_v \widehat{\Phi}_{\text{vdW}} + N_e \widehat{\Phi}_{\text{el}})}{r^2 G} dr \right]^{-1}, \quad (9)$$

where $\widehat{\Phi}_{\text{vdW}} = \Phi_{\text{vdW}}/A_H$ and $\widehat{\Phi}_{\text{el}} = \Phi_{\text{el}}/[q_1^2/(4\pi\epsilon_0 a_1)]$. Here, A_H is the Hamaker constant for the materials composing the two spheres and $\epsilon_0 = 8.85 \times 10^{-12} \text{ F m}^{-1}$ is the permittivity of vacuum. The dimensionless parameter $N_v = A_H/k_B T$ is called the Hamaker group that measures the relative strength of van der Waals interactions to Brownian diffusion and $N_e = q_1^2/(4\pi\epsilon_0 a_1 k_B T)$ measures the relative importance of electrostatic forces to Brownian motions.

B. Noncontinuum correction for the mobility function G

The hydrodynamic forces acting along the line of centers of two particles moving in a quiescent fluid are given by [10,54]

$$F_1 = -6\pi\mu_f a_1 [\Lambda_{11}(V_1 - V_2) + \Lambda_{12}V_2], \quad (10)$$

$$F_2 = -6\pi\mu_f a_2 [\Lambda_{21}(V_2 - V_1) + \Lambda_{22}V_2], \quad (11)$$

where V_i and F_i denote the velocity and forces on particles i , and Λ_{ij} is the dimensionless resistance coefficients representing the force on particle i because of the translational motion of particle j . From this the radial mobility function due to a central potential force or the Brownian diffusion can be expressed in terms of Λ_{ij} to be

$$G = \frac{1}{1 + \kappa} \frac{\Lambda_{12} + \kappa \Lambda_{22}}{\Lambda_{11} \Lambda_{22} + \Lambda_{21} \Lambda_{12}}. \quad (12)$$

Wang *et al.* [54] determined these resistance functions $\Lambda_{ij}(r, \kappa)$ by solving the Stokes equations for two spherical drops in bispherical coordinates (see Appendix A of Wang *et al.* [54] for details). To obtain the interactions between hard spheres, which is relevant to our study, we consider the case when the drop-to-medium viscosity ratio is infinite.

The first few terms in the series obtained from the bispherical coordinates solution accurately capture far-field continuum interactions. At close separations, using more terms in the series solution enhances accuracy. The series solutions with enough terms will emulate the continuum lubrication behavior of G . Batchelor [55] showed that $G \sim (1 + \kappa)^2 \xi / (2\kappa)$ for $\xi \rightarrow 0$ (here,

$\xi = r - 2$) which can be deduced from the fact that the resistance coefficients Λ_{11} and Λ_{21} diverge as $1/\xi$ in the lubrication region. Thus we can infer that making contact between two spheres with continuum hydrodynamics would take infinite time. Sundararajakumar and Koch [22] calculated the noncontinuum lubrication resistance and showed that it has a weaker divergence of $O(\ln[\ln(\text{Kn}/\xi)])$. Thus, noncontinuum lubrication interactions allow for contact in finite time. The noncontinuum lubrication resistance f^{nc} given in terms of rescaled radial separation, $\delta_0 = \xi/\text{Kn}$ and $t_0 = \ln(1/\delta_0) + 0.4513$, is [22,23]

$$f^{\text{nc}} = \begin{cases} \frac{\pi}{6} (\ln t_0 - t_0^{-1} - t_0^{-2} - 2t_0^{-3}) + 2.587\delta_0^2 + 1.419\delta_0 + 0.3847 & (\delta_0 < 0.26), \\ 5.607 \times 10^{-4} \delta_0^4 - 9.275 \times 10^{-3} \delta_0^3 + 6.067 \times 10^{-2} \delta_0^2 - 0.2082\delta_0 + 0.4654 + 0.05488\delta_0^{-1} & (0.26 < \delta_0 < 5.08), \\ -1.182 \times 10^{-4} \delta_0^3 + 3.929 \times 10^{-3} \delta_0^2 - 5.017 \times 10^{-2} \delta_0 + 0.3102 & (5.08 < \delta_0 < 10.55), \\ 0.0452[(6.649 + \delta_0) \ln(1 + 6.649\delta_0^{-1}) - 6.649] & (10.55 < \delta_0). \end{cases} \quad (13)$$

It is evident from (13) that for $\delta_0 \gg 1$, f^{nc} goes as $1/\xi$ (i.e., the continuum lubrication behavior). Also, the series solution for $\xi \ll 1$ approaches the continuum lubrication resistance. Thus the matched resistances Λ_{11} and Λ_{21} can be derived to be valid at all ξ and written as

$$\Lambda_{11} = \Lambda_{11}^{\text{bi}} - \Lambda_{11}^{\text{c}} + \Lambda_{11}^{\text{nc}}, \quad (14)$$

$$\Lambda_{21} = \Lambda_{21}^{\text{bi}} - \Lambda_{21}^{\text{c}} + \Lambda_{21}^{\text{nc}}, \quad (15)$$

where Λ_{11}^{bi} and Λ_{21}^{bi} are the series solution in bispherical coordinates performed by Wang *et al.* [54], Λ_{11}^{c} and Λ_{21}^{c} are continuum lubrication resistances, and Λ_{11}^{nc} and Λ_{21}^{nc} are noncontinuum lubrication resistances. These lubrication results are given as

$$\Lambda_{11}^{\text{c}} = \frac{2\kappa^2}{(1+\kappa)^3} \frac{1}{\xi} + c_0, \quad (16)$$

$$\Lambda_{21}^{\text{c}} = \frac{\Lambda_{11}^{\text{c}} - \Lambda_{12}}{\kappa}, \quad (17)$$

$$\Lambda_{11}^{\text{nc}} = \frac{2\kappa^2}{(1+\kappa)^3} \frac{f^{\text{nc}}}{\text{Kn}} + c_0, \quad (18)$$

$$\Lambda_{21}^{\text{nc}} = \frac{\Lambda_{11}^{\text{nc}} - \Lambda_{12}}{\kappa}, \quad (19)$$

where c_0 is a constant that is utilized to match the various regimes in order to get a smooth and uniformly valid resistance. We choose $\xi = 10^{-3}$ as a changeover separation distance between far-field and continuum lubrication. We evaluate c_0 such that $\Lambda_{11} = \Lambda_{11}^{\text{c}}$ at this transition point. Figure 2 shows how the mobility function G varies with the separation ξ when two spheres interact through noncontinuum hydrodynamics. To illustrate the difference, we plot the variation of G for full continuum hydrodynamic interactions. Recently, we have used uniformly valid forms of the axisymmetric hydrodynamic mobilities to study collisions of bidisperse spheres settling in an uniaxial compressional flow [23] and homogeneous isotropic turbulent flow [56].

III. RESULTS AND DISCUSSIONS

A. Collision efficiency without van der Waals and electrostatic forces ($N_v = 0$ and $N_e = 0$)

We determine the collision efficiency of aerosol particles that interact hydrodynamically but ignore the role of any interparticle potential (i.e., $\Phi = 0$). Of course, van der Waals and electrostatic interactions do exist between the aerosol particles. However, this calculation will demonstrate the effect of the breakdown of the continuum lubrication interactions on the collision dynamics of two Brownian particles. Without an interparticle potential, the expression for the collision efficiency

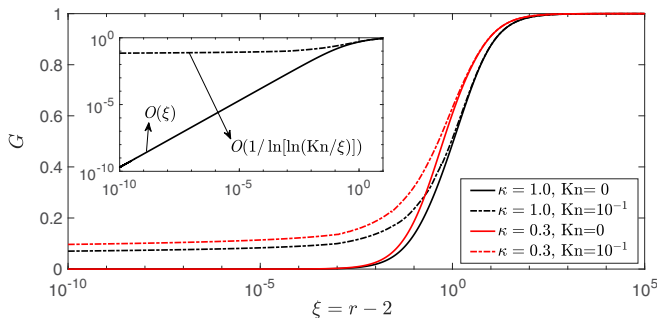


FIG. 2. The mobility functions G as a function of ξ when $\kappa = 0.3, 1.0$. The continuous lines are for continuum hydrodynamic interactions (i.e., $\text{Kn} = 0$) and the dashed-dotted lines are for noncontinuum lubrication interactions with $\text{Kn} = 10^{-1}$. The inset shows how G varies in the lubrication region due to continuum and noncontinuum hydrodynamic interactions when $\kappa = 1.0$.

becomes

$$E_{12} = \left(2 \int_0^\infty \frac{1}{(\xi + 2)^2 G} d\xi \right)^{-1}. \quad (20)$$

For rigid particles, the continuum lubrication interactions predict that $G = O(\xi)$ as $\xi \rightarrow 0$. Thus, the integral in (20) has a singularity for rigid spheres resulting in zero collision efficiency. However, the continuum assumption is no longer valid when the gap thickness between the surfaces of the two spheres is less than the mean free path of the medium. As discussed earlier, noncontinuum lubrication interactions lead to $G = O(1/\ln[\ln(\text{Kn}/\xi)])$, which decays slowly than its continuum counterpart so that the integral converges. This weaker noncontinuum lubrication force is valid for $\xi \leq O(\text{Kn})$ and is responsible for a finite collision rate even without colloidal forces. For drops, Davis *et al.* [57] showed that $G = O(\sqrt{\xi})$ for $\xi \ll 1$, which too decays slower than its rigid counterpart and thus results in finite collision times [53,58].

We perform the integral in (20) numerically using Gauss-Kronrod quadrature (the “quadgk” subroutine in *MATLAB*) with the ξ limit ranging from 10^{-10} to ∞ . Figure 3 shows how E_{12} varies with Kn for $\kappa = 0.3, 0.4, 0.5, 1.0$. The results will remain the same with κ being replaced by κ^{-1} since $G(\xi, \kappa) = G(\xi, \kappa^{-1})$. With decreasing Kn , E_{12} decreases because the reduction in non-continuum effects results in a higher lubrication resistance at small separations. For $\text{Kn} \rightarrow 0$ (corresponds to the full continuum hydrodynamic interactions), E_{12} will slowly approach zero. It is evident from Fig. 2 that the mobility function G deviates more from its continuum behavior when κ

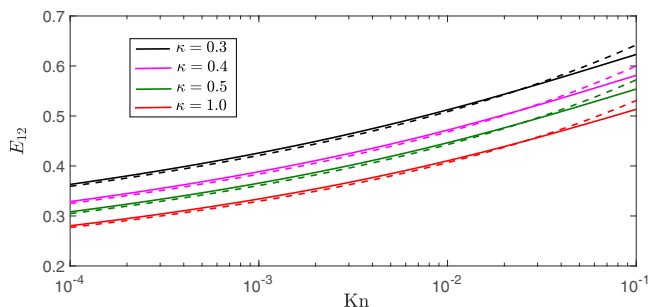


FIG. 3. The collision efficiency of Brownian particles as a function of the Knudsen number for different size ratios without interparticle potentials. The dashed lines are from the analytical expression (21), which are in good agreement with the numerical results.

is lower. Also, for lesser κ , the contribution of smaller particles to the relative Brownian diffusivity D_0 is more. Due to these two factors E_{12} is more for smaller κ as shown in Fig. 3. Inspired by Chun and Koch's [12] method for calculating the collision efficiency of two equal-sized particles, we can segregate the integral in Eq. (20) into contributions from the continuum, noncontinuum, and matching parts. This allows us to obtain the following analytical estimate for the collision efficiency for bidisperse spheres undergoing Brownian motion,

$$E_{12} \sim \left(c(\kappa) + \frac{\kappa}{(1 + \kappa)^2} \ln \left[\frac{1}{\text{Kn}} \right] \right)^{-1}, \quad (21)$$

where $c(\kappa)$ is a size-ratio dependent constant that must be obtained numerically. We can observe the favorable comparisons of the analytical expression with the numerically evaluated integral in Fig. 3. A useful fitting form for the constant is $c(\kappa) = (-0.7557\kappa^2 + 2.781\kappa + 1.716)/(\kappa + 1.861)$.

B. Collision efficiency with van der Waals forces, no electrostatic forces ($N_v \neq 0$ and $N_e = 0$)

While the relevance of electrostatic forces depends on the material of the aerosol particles and the charging mechanism, van der Waals forces caused by induced-dipole/induced-dipole interactions between the molecules constituting the particles will always be there. In this section, we will analyze the role of van der Waals interactions. The expression for the retarded van der Waals potential (Φ_{vdw}) is given in Appendix A. As we have noted in the previous section, the integral in (20) has a singularity for $\xi \rightarrow 0$ when particles interact through continuum hydrodynamics. However, the exponential term in the numerator of the integrand in Eq. (9) vanishes since the van der Waals potential approaches $-\infty$ as $\xi \rightarrow 0$, yielding a convergent result for the collision efficiency. Thus, one can get a finite result for the collision efficiency in the presence of van der Waals forces even if the continuum lubrication interactions dominate near contact. The coagulation between colloidal particles induced by Brownian motions and modulated by continuum hydrodynamic interactions and van der Waals attractions has been studied extensively [19]. From the discussion so far, we can conclude that either attractive interparticle forces (such as van der Waals forces) or noncontinuum lubrication effects are two mechanisms for overcoming the continuum lubrication forces at close separations. In actual cases, the relative importance of noncontinuum effects and van der Waals forces depends on various factors such as fluid pressures, sizes of particles, and aerosol materials. For example, noncontinuum effects predominantly drive the collision dynamics for aerosol particles in a low-pressure gas medium, and van der Waals interactions act as a dominant collision mechanism of colloidal particles in a liquid medium. In the current study, we evaluate the collision efficiency when both the factors are in play as they usually do for atmospheric aerosols.

In addition to Kn and κ , the collision efficiency with van der Waals interactions depends on the parameter $N_v = A_H/k_B T$. To estimate the typical values of N_v , we need the information of A_H . The values of A_H for several common materials are available in the literature (see Table 7.1 on p. 198 of Friendlander [2]). The dissolved ions inside can modify their Hamaker constant for haze drops even when the surrounding medium has no free ions. Mahanty and Ninham [59] quantified the modification of the Hamaker constant between two ionic drops in air. Dissolved ions inside the drops will decrease the nondispersive component of the Hamaker constant even when the intervening medium is air. However, there will be no screening effect on the interaction, unlike the van der Waals interaction of dielectric particles in an aqueous electrolyte medium. Yao and Capecehatro [60] mentioned that depending on the aerosol materials, the value of A_H can vary between 4×10^{-21} and 3×10^{-18} J. Therefore, N_v can approximately vary in the range 1–729 when $T = 298$ K. The typical values of N_v for water droplets, polystyrene, and metal particles are approximately 10, 20, and 100, respectively [12]. We calculate the collision efficiency for N_v values ranging from 10^{-2} to 10^2 . Though our theory can predict the collision efficiency for any value of $N_v \in [0, \infty)$, N_v values less than 1 are perhaps not achievable in actual experiments. The purpose of showing our results up to this small N_v is to demonstrate how pure noncontinuum hydrodynamics works. Recently, there have been studies that have illustrated that A_H can get reduced considerably for porous

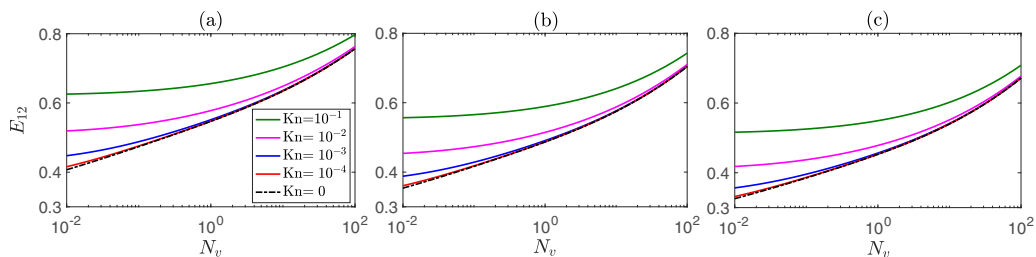


FIG. 4. The collision efficiency as a function of the parameter N_v for Brownian particles with different Kn and size ratios (a) $\kappa = 0.3$, (b) $\kappa = 0.5$, and (c) $\kappa = 1.0$. In these calculations, we assume $N_L = 10^2$. The color legend for (b) and (c) is the same as for (a). The black dashed-dotted lines in each of the three plots represent the collision efficiency due to continuum hydrodynamics (i.e., $\text{Kn} = 0$) in the presence of retarded van der Waals forces.

particles [61] and hollow particles [62], thus allowing for a possibility of accessing small values of N_v . Figure 4 quantitatively shows how van der Waals forces influence the collision dynamics of Brownian particles. For a given Kn and κ , the collision efficiency increases monotonically with increasing N_v . The van der Waals interactions play a dominant role for small Kn. In particular, when $\text{Kn} \leq 10^{-4}$, noncontinuum effects are less significant, and then van der Waals attractions solely drive the dynamics. Figure 4 proves this argument since $\text{Kn} = 0$ lines almost coincide with the $\text{Kn} = 10^{-4}$ lines. Physically, if Kn is small and N_v is large, van der Waals forces rapidly pull the particles into contact as they come close to each other. On the other hand, when Kn is relatively large, and $N_v \ll 1$ (i.e., weak van der Waals forces), E_{12} asymptotes to pure Brownian collision efficiency. However, it is important to note that the collision efficiency for continuum hydrodynamic interactions will asymptote to zero as $N_v \rightarrow 0$. As the previous case, the collisions are more efficient for particles with lesser κ . Figure 5 gives the variation of collision efficiency with Kn for $N_v = 0, 1, 10$, and 10^2 as the solid, dashed, dashed-dotted, and dotted lines, respectively. For $\text{Kn} < 10^{-2}$, the collision efficiencies for nonzero N_v are approximately independent of Kn. We expect that noncontinuum effects will dominate the collision dynamics when $\text{Kn} \geq O(1)$. For intermediate values of Kn, both noncontinuum lubrication flow and van der Waals forces influence the collision efficiency.

We calculate the collision efficiency as a function of κ under the action of different driving forces for small hydrocarbon particles with $a_1 = 0.5 \mu\text{m}$ and $a_1 = 1.0 \mu\text{m}$ (see Fig. 6). Taking the mean free path for air, $\lambda_0 \approx 0.1 \mu\text{m}$, Kn as a function of κ is given by $\text{Kn} = 0.2/(1 + \kappa)$ for $a_1 = 0.5 \mu\text{m}$ and $\text{Kn} = 0.4/(1 + \kappa)$ for $a_1 = 1.0 \mu\text{m}$. For hydrocarbon particles in air, $A_H \approx 5 \times 10^{-20} \text{J}$ (see Friendlander [2]), $\mu_f \approx 1.8 \times 10^{-5} \text{Pa s}$. We consider the air temperature $T = 298 \text{K}$. So, the

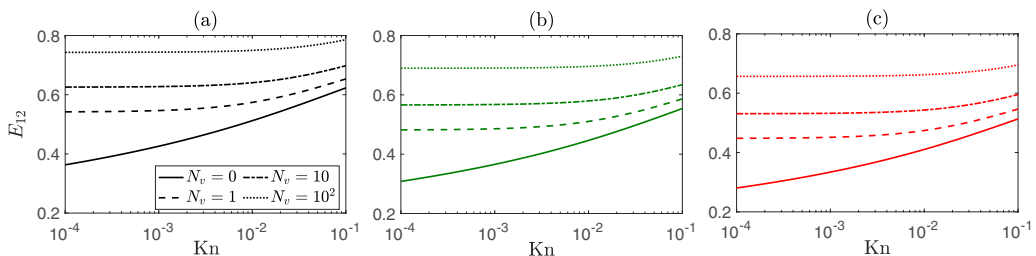


FIG. 5. The collision efficiency is plotted as a function of Kn for Brownian particles with different values of N_v and size ratios (a) $\kappa = 0.3$, (b) $\kappa = 0.5$, and (c) $\kappa = 1.0$. We assume $N_L = 125$ in these calculations. The legend for the line types of (b) and (c) is the same as for (a). The continuous lines in each of the three plots represent the collision efficiency due to pure noncontinuum hydrodynamics (i.e., $N_v = 0$).

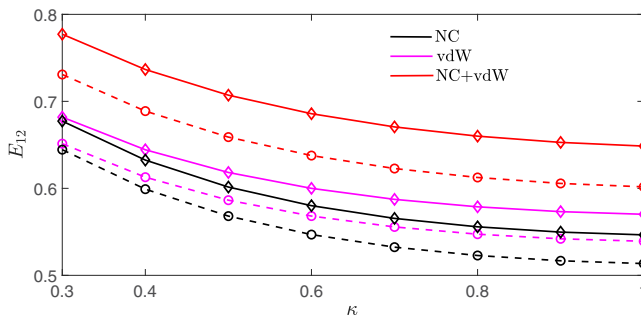


FIG. 6. The collision efficiency is plotted as a function of size ratio κ for tiny hydrocarbon particles. The solid lines with diamond markers are for $a_1 = 0.5 \mu\text{m}$, and the dashed lines with circle markers are for $a_1 = 1.0 \mu\text{m}$. The black, pink, and red colors represent the cases when driving mechanisms are only noncontinuum hydrodynamics (NC), only van der Waals forces (vdW), and combined effects of noncontinuum hydrodynamics and van der Waals forces (NC + vdW), respectively.

Hamaker group $N_v \approx 12.15$ and the dimensionless quantity N_L (see Appendix A for the definition of N_L) is given by $N_L = 10\pi(1 + \kappa)$ for $a_1 = 0.5 \mu\text{m}$ and $N_L = 20\pi(1 + \kappa)$ for $a_1 = 1.0 \mu\text{m}$. For a given κ , the collision efficiency due to noncontinuum lubrication interactions plus van der Waals attractions is highest and that due to only noncontinuum effects is lowest. The collision efficiency value due to van der Waals attractions when particles interact through continuum hydrodynamics lies in between these two cases. In all cases, the collision efficiency decreases monotonically with increasing κ and it is higher for the $a_1 = 0.5 \mu\text{m}$ case compared to the $a_1 = 1.0 \mu\text{m}$ case.

C. Collision efficiency with electrostatic forces ($N_e \neq 0$)

Electrostatic interactions between charged aerosol particles significantly impact many naturally occurring processes, such as droplet growth in the initial stage of rain formation. Let us consider $a_1 = 0.5 \mu\text{m}$ and the aerosol particle carrying electric charge in the range $1e < q_1 < 200e$. Thus, the parameter N_e capturing the relative strength of electrostatic force to Brownian motion can vary between $O(10^{-1})$ and $O(10^3)$. As discussed in Sec. I, two conductive spheres carrying charges of the same nature always attract each other at close separation except for certain combinations of size and charge ratio values. However, they always repel each other at moderate to large separations. The relative velocity is inward in the lubrication regime because the interaction force between the particle pair is always attractive there. As per the definition in (3), the relative velocity must be inward at all separations. Therefore, two spheres will come into contact if the sum of relative inward velocities induced by Brownian motions and van der Waals forces is higher than the relative outward velocity induced by electrostatic repulsion forces when interparticle separations are moderate to large. We find that the net relative velocity at the far-field is usually outward for particles with a relatively higher amount of charges on their surfaces, and thus they do not come into contact. Here, we aim to demonstrate the role of electrostatic interactions on collision dynamics separately. So, we estimate the collision efficiency for the hypothetical situation in which like-charged Brownian particles interact via noncontinuum hydrodynamics and electrostatic forces but experience no van der Waals force. However, towards the end of this section, we will present some results for physical systems where noncontinuum hydrodynamics, van der Waals, and electrostatic forces are in play. For collisions to occur without van der Waals forces (i.e., $N_v = 0$), Brownian motion-induced relative inward velocity must bring the particles into the attractive regime by overcoming the far-field repulsive electrostatic forces. We observe that depending on the values of κ , β , and N_e , the electrostatic interactions can either hinder or promote the collision dynamics of a pair of like-charged aerosols. Nonetheless, the collision efficiency must asymptotically match with the results for $N_e \rightarrow 0$ (Brownian diffusion dominated regime) and $N_e \rightarrow \infty$ (electrostatic forces

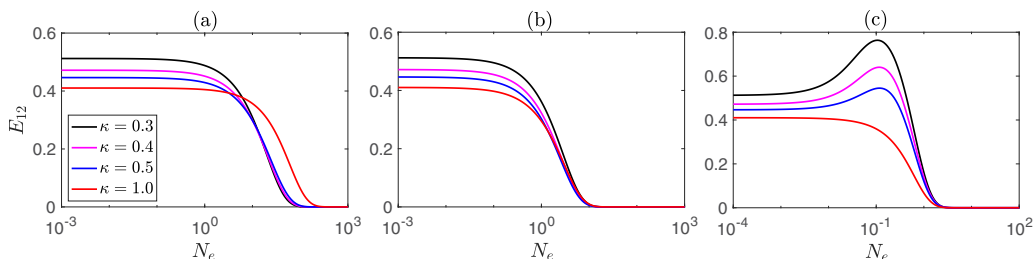


FIG. 7. The collision efficiency as a function of N_e , the relative strength of electrostatic forces to Brownian motion with different κ , and charge ratios (a) $\beta = 0.1$, (b) $\beta = 1$, and (c) $\beta = 10$ when $\text{Kn} = 10^{-2}$ and $N_v = 0$.

dominated regime). In the $N_e \rightarrow 0$ limit, E_{12} will approach Brownian collision efficiency due to noncontinuum hydrodynamics and for $N_e \rightarrow \infty$, E_{12} will approach zero. Similarly, in the presence of van der Waals interactions, E_{12} will asymptote to the result corresponding to noncontinuum hydrodynamics plus van der Waals forces when $N_e \rightarrow 0$.

Figure 7 shows the variation of the collision efficiency as a function of N_e for different κ , $\text{Kn} = 10^{-2}$, and $\beta = 0.1, 1, 10$ when $N_v = 0$. For smaller β values (for example, $\beta = 0.1$), the magnitude of the electrostatic attraction forces in close approach increases with increasing κ . This trend reverses gradually with increasing β , and it becomes the opposite when β is sufficiently high (for example, $\beta = 10$). Therefore, in the $N_e \gg 1$ limit, the collision efficiency must increase with increasing κ when β is small. On the other hand, we have reported in Sec. III A that the collision efficiency is higher for lesser κ when Brownian diffusion and noncontinuum hydrodynamic interactions drive the collision dynamics (i.e., $N_e \rightarrow 0$). Because of these two opposite behaviors in the two extreme regimes, the curves for different κ intersect with each other in intermediate N_e values when $\beta = 0.1$ [see Fig. 7(a)]. Also, for a given κ , the strength of the attraction forces is weak for smaller β , and thus the collision efficiency for this case is always smaller than the $N_e \rightarrow 0$ asymptotic value. The qualitative behaviors of the results are similar for β becoming ten times the previous β value. The only notable difference from the $\beta = 0.1$ results is that all the curves do not intersect with each other. For $\beta = 10$, the electrostatic attraction forces in the lubrication regime are so strong that the collision efficiency overshoots the pure noncontinuum result for some range of values of N_e when $\kappa = 0.3, 0.4, 0.5$ [see Fig. 7(c)]. As expected, in this case, the collision efficiencies are lower for higher κ . Since the electrostatic potential $\widehat{\Phi}_{\text{el}}$ has its maximum at some separation ξ_0 ($< \infty$) (where the force switches from a repulsive character to an attractive one), we use the Laplace method [63] to obtain the following asymptotic expression for the integral (9) when $N_e \gg 1$ and $N_v = 0$:

$$E_{12} \sim \frac{1}{2} \sqrt{\frac{N_e |\widehat{\Phi}_{\text{el}}''(\xi_0)|}{2\pi}} \xi_0^2 G(\xi_0) \exp[-N_e \widehat{\Phi}_{\text{el}}(\xi_0)]. \quad (22)$$

In the above expression $\widehat{\Phi}_{\text{el}}''(\xi_0)$ is the second-order derivative of $\widehat{\Phi}_{\text{el}}(\xi)$ with respect to ξ at $\xi = \xi_0$. The above analytical results for the $N_e \gg 1$ are in good agreement with the numerically obtained collision efficiencies, particularly when $\widehat{\Phi}_{\text{el}}$ have a pronounced peak. The above expression also suggests that the collision efficiency vanishes exponentially fast for large N_e .

To illustrate how collision efficiencies depend on the strength of noncontinuum hydrodynamics, we plot E_{12} as a function of N_e for different Kn when $\kappa = 0.5$, $\beta = 1$, and $N_v = 0$ (see Fig. 8). With decreasing N_e , E_{12} increases monotonically and asymptotes to the Brownian collision efficiency in the presence of noncontinuum hydrodynamics. As expected, the collision efficiency is higher for higher Kn . Unlike the van der Waals potentials, the electrostatic potential remains bounded at contact [see Eq. (B8)]. The $O(\xi^{-1})$ singularity of the integrand in (9) will remain when particles interact through continuum hydrodynamics in the presence of only electrostatic force. Therefore,

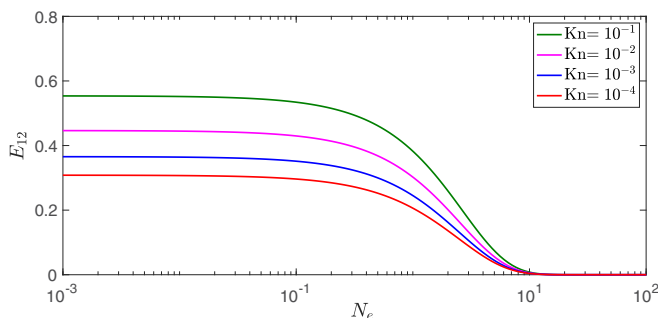


FIG. 8. The collision efficiency as a function of N_e for different Kn when $\kappa = 0.5$, $\beta = 1$, and $N_v = 0$.

the collisions between the particle pairs are not possible due to continuum hydrodynamics plus electrostatic interactions.

Figures 9(a) and 9(b) show contour plots for collision efficiencies of like-charged Brownian particles in the a_1 - q_1 parameter space when both noncontinuum hydrodynamics and electrostatic

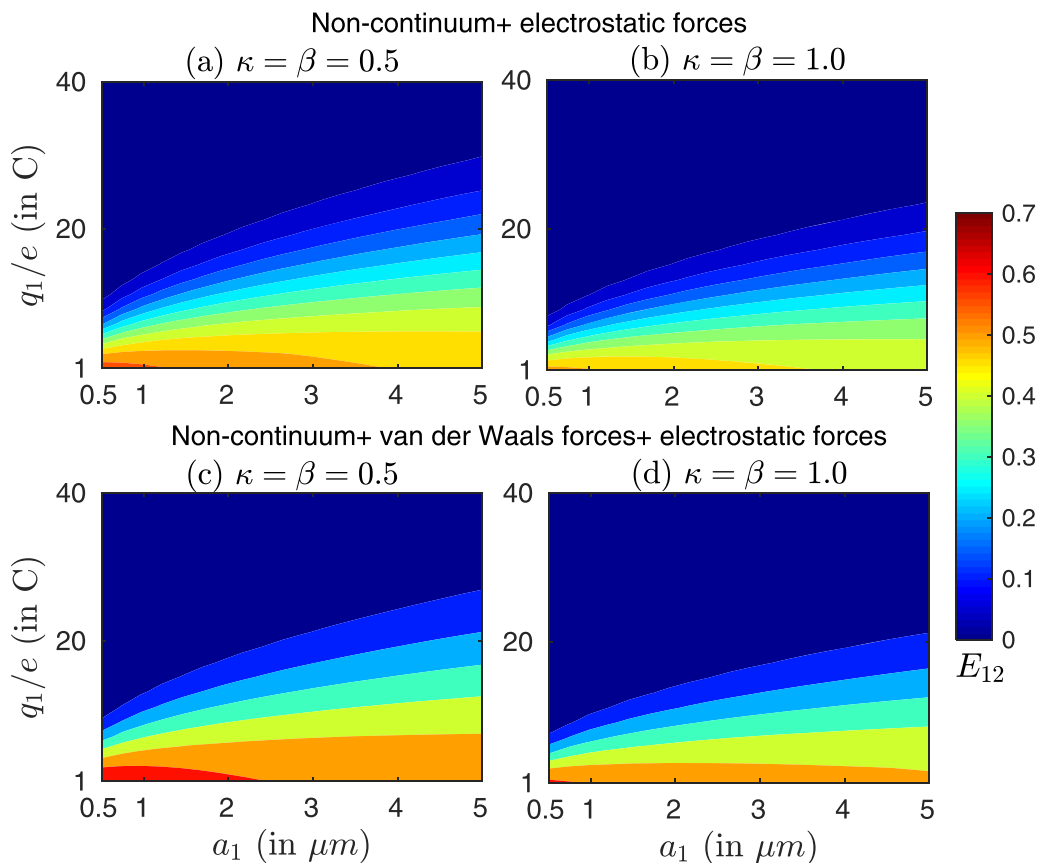


FIG. 9. The contour plot of collision efficiencies in the a_1 - q_1 parameter space. In (a) and (b) noncontinuum lubrication interactions plus electrostatic forces are considered. The van der Waals interactions are also incorporated in (c) and (d).

interactions are in play. In these plots, particle radii are in microns and particle charges (scaled by the elementary charge e) are in coulombs. We take $\lambda_0 = 0.1 \mu\text{m}$ for calculating the Knudsen number. So, we have $\text{Kn} = 2/(15a_1)$ when $\beta = 0.5$ and $\text{Kn} = 1/(10a_1)$ when $\beta = 1.0$. The required nondimensional parameter N_e does not depend on κ, β . For $T = 298 \text{ K}$, N_e is given by $N_e = 0.0561q_1^2/a_1$. Qualitatively both the plots are quite similar. For a given a_1 , the collision efficiency decreases with increasing q_1 and beyond a certain value of q_1 it becomes negligible. We find that these limiting values of q_1 are higher for larger a_1 . Collision efficiencies are negligible for larger q_1 because the electrostatic repulsion forces dominate the Brownian diffusion. Comparing between Figs. 9(a) and 9(b), we can say that collisions are more efficient for the $\kappa = \beta = 0.5$ case than for the $\kappa = \beta = 1.0$ case. We perform the above two calculations again after incorporating van der Waals forces [see Figs. 9(c) and 9(d)]. For calculations with van der Waals interactions, we take $N_v = 12.15$ (the same as stated in Sec. III B). The dimensionless parameter N_L is given by $N_L = 30\pi a_1$ for $\kappa = 0.5$ and $N_L = 40\pi a_1$ for $\kappa = 1.0$. As expected, collision efficiencies are higher in the presence of van der Waals forces. However, the qualitative trends of the collision efficiencies are quite similar.

IV. CONCLUSIONS

We have studied the coagulation rate of a pair of spherical particles experiencing Brownian diffusion, both with and without interparticle forces. The present analysis considers noncontinuum hydrodynamics that plays a crucial role in particle collisions in gaseous media. The noncontinuum lubrication interactions result in finite collision rates even without attractive nonhydrodynamic forces. This finding contrasts the well-known prediction that continuum lubrication forces do not allow surface-to-surface contact between rigid spheres. We have used the uniformly valid solution of the axisymmetric mobility function (G) that captures the noncontinuum lubrication at near-field and continuum hydrodynamic interactions for moderate to large separations. We find that the collision efficiencies increase monotonically with increasing the noncontinuum effects (i.e., increasing Kn).

We have also performed the collision efficiency calculations in the presence of retarded van der Waals potentials and electrostatic forces. The van der Waals forces are always attractive and thus enhance the collision efficiency. In Sec. III B, we have presented how collision efficiency varies with the size ratio, the Knudsen number, and the relative strength of van der Waals forces to Brownian diffusion. Depending on the size ratio, charge ratio, and dimensionless center-to-center distance values, the electrostatic interaction force between two like-charged conducting spheres can be attractive, zero, or repulsive. Unlike the van der Waals forces, electrostatic interaction forces can either diminish or enhance the collision efficiency. We have shown how collision efficiencies vary in the size ratio–charge ratio parameter space when noncontinuum effects, van der Waals, and electrostatic interactions are in play. One can utilize the present study to predict how the particle size distribution evolves with time and then compare it with experiments. To solve this evolution equation, one requires accurate estimation for the collision rate constant.

Almost all previous studies, including the present one, have treated charged aerosol particles as perfect conductors. The actual collision rate might differ from the present one due to this assumption since dielectric constants for aerosol materials are finite. The deviation from the actual collision rate will be even more for haze droplets whose dielectric constant is approximately 80 at STP. Most importantly, the difference in electrostatic forces between dielectric and perfect conducting spheres becomes more prominent at close separations where noncontinuum hydrodynamics becomes dominant. Therefore, in the lubrication regime, the collision dynamics of dielectric spherical pairs are expected to be significantly different from that of a perfect conductor case. We plan to address this issue in a forthcoming study. Two like-charged dielectric spheres, analogous to perfect conductors, can also attract each other in close separations. The combinations of charge ratio and size ratio values for which two dielectric spheres repel each other near contact form a bandlike region in the β - κ parameter space (see Bichoutskaia *et al.* [64] and Khachatourian *et al.* [65]), whereas in the case of a pair of perfect conducting spheres, this region becomes a single curve [Eq. (2)]. Thus a future extension of our study needs to consider an additional parameter, the dielectric constant for aerosol particles, for calculating the collision efficiency.

The current study ignores the role of sedimentation in the collision of aerosol particles. Dhanasekaran *et al.* [23] studied the gravity-induced coagulation rate due to noncontinuum lubrication interactions, ignoring Brownian motion. Many previous studies have investigated the role of electrostatic forces on collisions between like-charged conducting spheres settling due to gravity in a quiescent environment [48,66]. In reality, both Brownian diffusion and gravitational settling would act in tandem during collisions of micron-sized particles. With the inclusion of gravitational effects, the problem loses its isotropic nature, and thus we need to solve the advection-diffusion equation for the pair probability for arbitrary Pe. In the continuum limit, when van der Waals forces and/or interfacial mobility induce collisions, Zinchenko and Davis [10] considered the arbitrary Pe problem. Similarly, we can extend the current analytical approach of finding the Pe = 0 collision rate to include the effects of sedimentation. The numerical solution of the advection-diffusion equation would need special attention in such a scenario to account for the presence of the diffusive boundary layer near the collision sphere [67] at large Pe.

ACKNOWLEDGMENTS

Financial support for this work was provided by the Prime Minister's Research Fellows (PMRF) scheme, Ministry of Education, Government of India. P.P. would like to thank Dr. J. Dhanasekaran for sharing the code for the uniformly valid hydrodynamic mobility function. A.R. would like to acknowledge the support from the Laboratory for Atmospheric and Climate Sciences, Indian Institute of Technology Madras, India.

APPENDIX A: THE POTENTIAL FOR RETARDED VAN DER WAALS INTERACTION BETWEEN TWO SPHERES

Most collision rate calculations use the unretarded form of the van der Waals potential derived by Hamaker [68] using a pairwise additivity theory. Hamaker's calculation does not consider the retardation due to the finite propagation speed of electromagnetic waves. For interparticle separations comparable to or greater than the London wavelength λ_L ($\approx 0.1 \mu\text{m}$), the effects of retardation must be taken into account [19]. We have utilized the work of Zinchenko and Davis [10] who obtained the retarded van der Waals potential (Φ_{vdw}) by analytically integrating the dispersion energy between two molecules. The retarded van der Waals potential is given by

$$\begin{aligned} \Phi_{\text{vdw}} = & -\frac{A_H}{3\xi} \frac{\kappa}{(1+\kappa)^2} \frac{1}{1+1.769p_0} \mathcal{H}(0.5-p_0) \\ & -\frac{A_H}{60} \left[2.45\Psi J_7 - \frac{2.17}{12} \Psi^2 J_8 + \frac{0.59}{168} \Psi^3 J_9 \right] \mathcal{H}(p_0-0.5), \end{aligned} \quad (\text{A1})$$

where $p_0 = 0.5N_L\xi$ and $\Psi = 4/(rN_L)$ with N_L being the radius of the two particles scaled by the London wavelength λ_L [i.e., $N_L = 2\pi(a_1+a_2)/\lambda_L = 2\pi a_1(1+\kappa)/\lambda_L$]. The \mathcal{H} is the Heaviside step function. The expressions for the coefficients J_n are given by [10]

$$\begin{aligned} J_n = & (n-6)! \left[\frac{1}{(1-\alpha_1-\alpha_2)^{n-5}} + \frac{1}{(1+\alpha_1+\alpha_2)^{n-5}} + \frac{1}{(1+\alpha_1-\alpha_2)^{n-5}} + \frac{1}{(1-\alpha_1+\alpha_2)^{n-5}} \right] \alpha_1 \alpha_2 \\ & + (n-7)! \left[\frac{\alpha_1-\alpha_2}{(1-\alpha_1+\alpha_2)^{n-6}} + \frac{\alpha_2-\alpha_1}{(1+\alpha_1-\alpha_2)^{n-6}} + \frac{\alpha_1+\alpha_2}{(1+\alpha_1+\alpha_2)^{n-6}} - \frac{\alpha_1+\alpha_2}{(1-\alpha_1-\alpha_2)^{n-6}} \right] \\ & + f_n(\alpha_1+\alpha_2) + f_n(-\alpha_1-\alpha_2) - f_n(\alpha_2-\alpha_1) - f_n(\alpha_1-\alpha_2), \end{aligned} \quad (\text{A2})$$

where $\alpha_1 = 2/(1+\kappa)$, $\alpha_2 = 2\kappa/(1+\kappa)$, and

$$f_n(x) = -\ln(1+x) \quad \text{for } n = 7, \quad (\text{A3})$$

$$f_n(x) = \frac{(n-8)!}{(1+x)^{n-7}} \quad \text{for } n \geq 8. \quad (\text{A4})$$

The above van der Waals interaction energy switches between the two well-known limits, the London interaction in the near-field and the Casimir-Polder interaction in the far-field, and Hamaker's additive approach is implemented. An exact approach to calculating the interaction energy would require the solution of Maxwell's equations in the two-sphere geometry, accounting for the material properties. Pailthorpe and Russel [69] had addressed this by revisiting the multipole expansion approach of Langbein [70], improving the convergence issues. The expressions thus obtained are typically cumbersome to implement in numerical calculations. Vanni and Baldi [71] have shown that for a nonconducting medium, the difference between the rigorous result and the modified Hamaker approach is negligible; differences become substantial for an electrolyte medium. There have been recent attempts at computing the van der Waals/Casimir forces between objects by solving the electrodynamic equations using scattering theory [72,73].

APPENDIX B: THE ELECTROSTATIC INTERACTION POTENTIAL

The interaction potential of two charged conducting spheres can be written as

$$\Phi_{\text{el}} = \frac{q_1^2}{4\pi\epsilon_0 a_1} \widehat{\Phi}_{\text{el}}, \quad (\text{B1})$$

where $\widehat{\Phi}_{\text{el}}$ is the nondimensional interaction potential. We define the $\widehat{\Phi}_{\text{el}}$ in such a way that it becomes zero when the separation distance between the spheres is infinite. Therefore, we have

$$\widehat{\Phi}_{\text{el}} = \widehat{W} - \widehat{W}_\infty, \quad (\text{B2})$$

where \widehat{W} and \widehat{W}_∞ are respectively the electrostatic potential energy of two spherical conductors for arbitrary and infinite separation. The expression of \widehat{W} for two spheres having constant surface charges is given by [31]

$$\widehat{W} = \frac{\beta^2 S_{11} - 2\beta S_{12} + S_{22}}{2(S_{11}S_{22} - S_{12}^2)}, \quad (\text{B3})$$

where S_{11} , S_{12} , and S_{22} are the dimensionless (nondimensionalized by $4\pi\epsilon_0 a_1$) capacitance coefficients. The explicit expressions for these coefficients are [31,74]

$$S_{11} = \kappa \sinh \eta \sum_{n=1}^{\infty} [\kappa \sinh n\eta + \sinh(n-1)\eta]^{-1}, \quad (\text{B4})$$

$$S_{22} = \kappa \sinh \eta \sum_{n=1}^{\infty} [\sinh n\eta + \kappa \sinh(n-1)\eta]^{-1}, \quad (\text{B5})$$

$$S_{12} = -\frac{2\kappa}{r(1+\kappa)} \sinh \eta \sum_{n=1}^{\infty} [\sinh n\eta]^{-1}. \quad (\text{B6})$$

The dimensionless parameter η in terms of nondimensional separation and size ratio is given by

$$\eta = \cosh^{-1} \left[\frac{(1+\kappa)^2 r^2 - 4 - 4\kappa^2}{8\kappa} \right]. \quad (\text{B7})$$

Lekner [31] also derived the analytical expression for the potential energy in the lubrication regime (i.e., $\xi \rightarrow 0$) by expanding the capacitance coefficients. The near-field form of \widehat{W} at $O(\xi)$ is given by

$$\begin{aligned} \widehat{W} \sim & -\left(\frac{1+\kappa}{2\kappa}\right) \\ & \times \frac{(1+\beta)^2 \ln \{4\kappa/[(1+\kappa)^2 \xi]\} + 4\beta\gamma - 2\beta^2 \psi[\kappa/(1+\kappa)] - 2\psi[1/(1+\kappa)]}{\{2\gamma + \psi[\kappa/(1+\kappa)] + \psi[1/(1+\kappa)]\} \ln \{4\kappa/[(1+\kappa)^2 \xi]\} + 2\gamma^2 - 2\psi[\kappa/(1+\kappa)]\psi[1/(1+\kappa)]}. \end{aligned} \quad (\text{B8})$$

We can neglect the electrostatic interaction when the separation distance between the spheres is large. Thus the potential energy in the $\xi \rightarrow \infty$ limit becomes

$$\begin{aligned} W_\infty &= \frac{1}{4\pi\epsilon_0} \left(\frac{q_1^2}{2a_1} + \frac{q_2^2}{2a_2} \right) \\ &= \frac{q_1^2}{4\pi\epsilon_0 a_1} \frac{1}{2} \left(\frac{\beta^2}{\kappa} + 1 \right). \end{aligned} \quad (\text{B9})$$

So, the expression of \widehat{W}_∞ is

$$\widehat{W}_\infty = \frac{1}{2} \left(\frac{\beta^2}{\kappa} + 1 \right). \quad (\text{B10})$$

-
- [1] H. R. Pruppacher and J. D. Klett, *Microphysics of Clouds and Precipitation: Reprinted 1980* (Springer, Berlin, 2012).
- [2] S. K. Friedlander, *Smoke, Dust and Haze: Fundamentals of Aerosol Dynamics* (Oxford University Press, London, 2000).
- [3] R. A. Shaw, Particle-turbulence interactions in atmospheric clouds, *Annu. Rev. Fluid Mech.* **35**, 183 (2003).
- [4] W. W. Grabowski and L.-P. Wang, Growth of cloud droplets in a turbulent environment, *Annu. Rev. Fluid Mech.* **45**, 293 (2013).
- [5] M. Balthasar, F. Mauss, A. Knobel, and M. Kraft, Detailed modeling of soot formation in a partially stirred plug flow reactor, *Combust. Flame* **128**, 395 (2002).
- [6] M. V. Smoluchowski, Versuch einer mathematischen Theorie der Koagulationskinetik kolloider Lösungen, *Z. Phys. Chem.* **92U**, 129 (1918).
- [7] L. A. Spielman, Viscous interactions in Brownian coagulation, *J. Colloid Interface Sci.* **33**, 562 (1970).
- [8] I. A. Valioulis and E. J. List, Collision efficiencies of diffusing spherical particles: Hydrodynamic, van der Waals and electrostatic forces, *Adv. Colloid Interface Sci.* **20**, 1 (1984).
- [9] S. Kim and C. F. Zukoski, A model of growth by hetero-coagulation in seeded colloidal dispersions, *J. Colloid Interface Sci.* **139**, 198 (1990).
- [10] A. Z. Zinchenko and R. H. Davis, Gravity-induced coalescence of drops at arbitrary Péclet numbers, *J. Fluid Mech.* **280**, 119 (1994).
- [11] J. Chun and D. L. Koch, Coagulation of monodisperse aerosol particles by isotropic turbulence, *Phys. Fluids* **17**, 027102 (2005).
- [12] J. Chun and D. L. Koch, The effects of non-continuum hydrodynamics on the Brownian coagulation of aerosol particles, *J. Aerosol Sci.* **37**, 471 (2006).
- [13] N. A. Fuchs, *The Mechanics of Aerosols* (Pergamon, New York, 1964).
- [14] M. Sitarski and J. H. Seinfeld, Brownian coagulation in the transition regime, *J. Colloid Interface Sci.* **61**, 261 (1977).
- [15] P. E. Wagner and M. Kerker, Brownian coagulation of aerosols in rarefied gases, *J. Chem. Phys.* **66**, 638 (1977).
- [16] S. N. Shon, G. Kasper, and D. T. Shaw, An experimental study of Brownian coagulation in the transition regime, *J. Colloid Interface Sci.* **73**, 233 (1980).
- [17] G. Narsimhan and E. Ruckenstein, The Brownian coagulation of aerosols over the entire range of Knudsen numbers: Connection between the sticking probability and the interaction forces, *J. Colloid Interface Sci.* **104**, 344 (1985).
- [18] D. S. Kim, S. H. Park, Y. M. Song, D. H. Kim, and K. W. Lee, Brownian coagulation of polydisperse aerosols in the transition regime, *J. Aerosol Sci.* **34**, 859 (2003).
- [19] W. B. Russel, D. Saville, and W. R. Schowalter, *Colloidal Dispersions*, Cambridge Monographs on Mechanics (Cambridge University Press, Cambridge, UK, 1989).

- [20] L. M. Hocking, The effect of slip on the motion of a sphere close to a wall and of two adjacent spheres, *J. Eng. Math.* **7**, 207 (1973).
- [21] R. H. Davis, The rate of coagulation of a dilute polydisperse system of sedimenting spheres, *J. Fluid Mech.* **145**, 179 (1984).
- [22] R. R. Sundararajakumar and D. L. Koch, Non-continuum lubrication flows between particles colliding in a gas, *J. Fluid Mech.* **313**, 283 (1996).
- [23] J. Dhanasekaran, A. Roy, and D. L. Koch, Collision rate of bidisperse spheres settling in a compressional non-continuum gas flow, *J. Fluid Mech.* **910**, A10 (2021).
- [24] S. E. Devir, On the coagulation of aerosols (part I), *J. Colloid Sci.* **18**, 744 (1963).
- [25] S. E. Devir, On the coagulation of aerosols III. Effect of weak electric charges on rate, *J. Colloid Interface Sci.* **23**, 80 (1967).
- [26] N. Gavish and K. Promislow, Dependence of the dielectric constant of electrolyte solutions on ionic concentration: A microfield approach, *Phys. Rev. E* **94**, 012611 (2016).
- [27] E. B. Lindgren, H.-K. Chan, A. J. Stace, and E. Besley, Progress in the theory of electrostatic interactions between charged particles, *Phys. Chem. Chem. Phys.* **18**, 5883 (2016).
- [28] T. B. Jones, *Electromechanics of Particles* (Cambridge University Press, Cambridge, UK, 2005).
- [29] M. H. Davis, Two charged spherical conductors in a uniform electric field: Forces and field strength, *Q. J. Mech. Appl. Math.* **17**, 499 (1964).
- [30] A. Russell, The coefficients of capacity and the mutual attractions or repulsions of two electrified spherical conductors when close together, *Proc. R. Soc. London, Ser. A* **82**, 524 (1909).
- [31] J. Lekner, Electrostatics of two charged conducting spheres, *Proc. R. Soc. A* **468**, 2829 (2012).
- [32] J. Lekner, Regions of attraction between like-charged conducting spheres, *Am. J. Phys.* **84**, 474 (2016).
- [33] J. C. Maxwell, *A Treatise on Electricity and Magnetism*, Vol. 1 (Clarendon Press, Oxford, UK, 1873).
- [34] L. D. Landau and E. Lifshitz, *Electrodynamics of Continuous Media*, Vol. 8 (Elsevier, Amsterdam, 2013).
- [35] A. S. Khair, Electrostatic forces on two almost touching nonspherical charged conductors, *J. Appl. Phys.* **114**, 134906 (2013).
- [36] S. Banerjee, T. Peters, N. Brown, and Y. Song, Exact closed-form and asymptotic expressions for the electrostatic force between two conducting spheres, *Proc. R. Soc. A* **477**, 20200866 (2021).
- [37] V. Munirov and A. Filippov, Interaction of two dielectric macroparticles, *J. Exp. Theor. Phys.* **117**, 809 (2013).
- [38] A. V. Khachatourian and A. O. Wistrom, Size effects in aerosol electrostatic interactions, *J. Colloid Interface Sci.* **242**, 52 (2001).
- [39] D. D. Huang, J. H. Seinfeld, and K. Okuyama, Image potential between a charged particle and an uncharged particle in aerosol coagulation—enhancement in all size regimes and interplay with van der Waals forces, *J. Colloid Interface Sci.* **141**, 191 (1991).
- [40] J. Lu, H. Nordsiek, E. W. Saw, and R. A. Shaw, Clustering of Charged Inertial Particles in Turbulence, *Phys. Rev. Lett.* **104**, 184505 (2010).
- [41] Y. Yao and J. Capecelatro, Competition between drag and coulomb interactions in turbulent particle-laden flows using a coupled-fluid–Ewald-summation based approach, *Phys. Rev. Fluids* **3**, 034301 (2018).
- [42] W. C. Hinds, *Aerosol Technology: Properties, Behavior, and Measurement of Airborne Particles* (Wiley, Hoboken, NJ, 1999).
- [43] Y. Kousaka, K. Okuyama, M. Adachi, and K. Ebie, Measurement of electric charge of aerosol particles generated by various methods, *J. Chem. Eng. Jpn.* **14**, 54 (1981).
- [44] C.-J. Tsai, J.-S. Lin, C. G. Deshpande, and L.-C. Liu, Electrostatic charge measurement and charge neutralization of fine aerosol particles during the generation process, *Part. Part. Syst. Charact.* **22**, 293 (2005).
- [45] K. Ghosh, S. N. Tripathi, M. Joshi, Y. S. Mayya, A. Khan, and B. K. Sapra, Modeling studies on coagulation of charged particles and comparison with experiments, *J. Aerosol Sci.* **105**, 35 (2017).
- [46] A. A. Onischuk, S. di Stasio, V. V. Karasev, A. M. Baklanov, G. A. Makhov, A. L. Vlasenko, A. R. Sadykova, A. V. Shipovalov, and V. N. Panfilov, Evolution of structure and charge of soot aggregates during and after formation in a propane/air diffusion flame, *J. Aerosol Sci.* **34**, 383 (2003).

- [47] M. M. Maricq, The dynamics of electrically charged soot particles in a premixed ethylene flame, *Combust. Flame* **141**, 406 (2005).
- [48] B. A. Tinsley, R. P. Rohrbaugh, M. Hei, and K. V. Beard, Effects of image charges on the scavenging of aerosol particles by cloud droplets and on droplet charging and possible ice nucleation processes, *J. Atmos. Sci.* **57**, 2118 (2000).
- [49] B. Ellasson, W. Egli, J. R. Ferguson, and H. Jodeit, Coagulation of bipolarly charged aerosols in a stack coagulator, *J. Aerosol Sci.* **18**, 869 (1987).
- [50] S. Dhanorkar and A. K. Kamra, Effect of coagulation on the particle charge distribution and air conductivity, *J. Geophys. Res.: Atmos.* **106**, 12055 (2001).
- [51] M. P. Simones and S. K. Loyalka, Measurements of charged aerosol coagulation, *Nucl. Technol.* **189**, 45 (2015).
- [52] M. P. Simones, S. K. Loyalka, C. Duffy, R. MacLoughlin, A. Tatham, and P. Power, Measurement of the size and charge distribution of sodium chloride particles generated by an Aeroneb Pro® pharmaceutical nebulizer, *Eur. J. Nanomed.* **6**, 29 (2014).
- [53] X. Zhang and R. H. Davis, The rate of collisions due to Brownian or gravitational motion of small drops, *J. Fluid Mech.* **230**, 479 (1991).
- [54] H. Wang, A. Z. Zinchenko, and R. H. Davis, The collision rate of small drops in linear flow fields, *J. Fluid Mech.* **265**, 161 (1994).
- [55] G. K. Batchelor, Brownian diffusion of particles with hydrodynamic interaction, *J. Fluid Mech.* **74**, 1 (1976).
- [56] J. Dhanasekaran, A. Roy, and D. L. Koch, Collision rate of bidisperse, hydrodynamically interacting spheres settling in a turbulent flow, *J. Fluid Mech.* **912**, A5 (2021).
- [57] R. H. Davis, J. A. Schonberg, and J. M. Rallison, The lubrication force between two viscous drops, *Phys. Fluids* **1**, 77 (1989).
- [58] A. Z. Zinchenko and R. H. Davis, Collision rates of spherical drops or particles in a shear flow at arbitrary Peclet numbers, *Phys. Fluids* **7**, 2310 (1995).
- [59] J. Mahanty and B. W. Ninham, *Dispersion Forces*, Vol. 1 (Academic, Cambridge, MA, 1976).
- [60] Y. Yao and J. Capecehatro, Deagglomeration of cohesive particles by turbulence, *J. Fluid Mech.* **911**, A10 (2021).
- [61] E. Y. Santiago, J. Pérez-Rodríguez, and R. Esquivel-Sirvent, Dispersive properties of mesoporous gold: van der Waals and near-field radiative heat interactions, *J. Phys. Chem. C* **121**, 12392 (2017).
- [62] C. Shen, S. A. Bradford, M. Flury, Y. Huang, Z. Wang, and B. Li, DLVO interaction energies for hollow particles: The filling matters, *Langmuir* **34**, 12764 (2018).
- [63] C. M. Bender and S. A. Orszag, *Advanced Mathematical Methods for Scientists and Engineers I: Asymptotic Methods and Perturbation Theory* (Springer, Berlin, 2013).
- [64] E. Bichoutskaia, A. L. Boatwright, A. Khachatourian, and A. J. Stace, Electrostatic analysis of the interactions between charged particles of dielectric materials, *J. Chem. Phys.* **133**, 024105 (2010).
- [65] A. Khachatourian, H.-K. Chan, A. J. Stace, and E. Bichoutskaia, Electrostatic force between a charged sphere and a planar surface: A general solution for dielectric materials, *J. Chem. Phys.* **140**, 074107 (2014).
- [66] A. Khain, V. Arkhipov, M. Pinsky, Y. Feldman, and Y. Ryabov, Rain enhancement and fog elimination by seeding with charged droplets. Part I: Theory and numerical simulations, *J. Appl. Meteorol.* **43**, 1513 (2004).
- [67] J. Wen and G. K. Batchelor, The rate of coagulation in a dilute suspension of small particles, *Sci. China, Ser. A: Math., Phys., Astron. Technol. Sci.* **28**, 172 (1985).
- [68] H. Hamaker, The London–van der Waals attraction between spherical particles, *Physica* **4**, 1058 (1937).
- [69] B. Pailthorpe and W. Russel, The retarded van der Waals interaction between spheres, *J. Colloid Interface Sci.* **89**, 563 (1982).
- [70] D. Langbein, Theory of van der Waals Attraction, *Springer Tracts in Modern Physics Vol. 72* (Springer, Berlin, 1974), pp. 1–139.

- [71] M. Vanni and G. Baldi, Coagulation efficiency of colloidal particles in shear flow, [Adv. Colloid Interface Sci.](#) **97**, 151 (2002).
- [72] S. J. Rahi, T. Emig, N. Graham, R. L. Jaffe, and M. Kardar, Scattering theory approach to electrodynamic Casimir forces, [Phys. Rev. D](#) **80**, 085021 (2009).
- [73] B. Spreng, P. A. Maia Neto, and G.-L. Ingold, Plane-wave approach to the exact van der Waals interaction between colloid particles, [J. Chem. Phys.](#) **153**, 024115 (2020).
- [74] J. Lekner, Capacitance coefficients of two spheres, [J. Electrostat.](#) **69**, 11 (2011).